Time-Resolved Dynamics of Mercury Uptake, Methylmercury Production, and Export by Pseudodesulfovibrio hydrargyri BerOc1 at Different Mercury Concentrations

Maureen Le Bars, Mathilde Monperrus, Sophie Barrouilhet, Mélina Petrel, Marisol Goñi, Marie-Pierre Isaure

ACS EARTH AND SPACE CHEMISTRY

http://pubs.acs.org/journal/aesccq
Article

Time-Resolved Dynamics of Mercury Uptake, Methylmercury Production, and Export by *Pseudodesulfovibrio hydrargyri* BerOc1 at Different Mercury Concentrations

Maureen Le Bars,* Mathilde Monperrus, Sophie Barrouilhet, Melina Petrel, Marisol Goñi-Urriza, and Marie-Pierre Isaure*

Cite This: https://doi.org/10.1021/acsearthspacechem.4c00327
Read Online

ABSTRACT: Methylmercury (MeHg) is highly toxic and is mainly produced in anoxic environments by certain microorganisms. Net MeHg production involves a series of separate cellular processes: the uptake of inorganic divalent Hg (Hg(II)) by the cell, intracellular enzymatic Hg(II) methylation, and the release of MeHg into the extracellular medium, as well as MeHg demethylation. As a biological process, saturation at the cellular level can be anticipated at all stages of the Hg transformation. The aim of this study was to investigate the kinetics of Hg(II) methylation and MeHg demethylation over a 24-h period in the model sulfate-reducing strain *Pseudodesulfovibrio hydrargyri* BerOc1, across a range of Hg(II) concentrations from 0.03 to 3.15 μM. The distribution of Hg(II) and MeHg over 24 h within three cellular fractions (extracellular, adsorbed to the cells, and intracellular) was determined to estimate Hg uptake and export. With increasing Hg(II) concentrations, we observed (i) an increase in the accumulated intracellular Hg(II), (ii) a reduction in the methylation rate, and (iii) an increase in MeHg associated with the cells after a short Hg(II) exposure time (<1 h). Our study suggests that the saturation of MeHg production is likely not driven by Hg(II) uptake but rather by Hg(II) intracellular speciation, Hg(II) methylation by HgcAB proteins, and/or MeHg export. These results are essential to better predict and understand the parameters influencing MeHg production within more complex environments, such as anoxic sediments and soils.

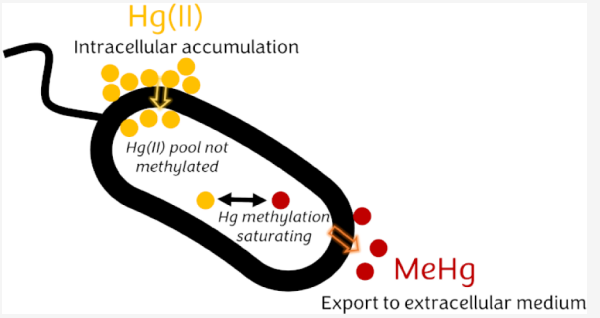

KEYWORDS: *mercury, methylation, demethylation, intracellular accumulation, kinetic rates, uptake, export, Hg*

1. INTRODUCTION

Methylmercury (MeHg), a potent neurotoxin, is produced from inorganic divalent mercury (Hg(II)) by certain anaerobic microorganisms. These known Hg(II) methylators include sulfate-reducing, iron-reducing, syntrophic *Desulfobacterota*, methanogens, and *Firmicutes*.[1−3] Recent metagenomic analyses[4−6] suggest that the diversity of putative methylators is much higher than currently known, including some microaerophilic microorganisms.[7] Once biotically produced, MeHg undergoes bioaccumulation and biomagnification within the food chain,[8] leading to human and wildlife MeHg exposure through fish[9] or rice consumption.[10] To accurately predict and mitigate MeHg exposure in humans and wildlife, it is crucial to understand the underlying mechanisms responsible for Hg(II) methylation, particularly at the microbial cell level. In our previous studies, we proposed that MeHg production by the sulfate-reducing bacterium (SRB) *Pseudodesulfovibrio hydrargyri* BerOc1 is a saturating process.[11,12] This conclusion was drawn based on the observed decrease in methylation potential (MeHg/total Hg) as the initial concentration of Hg(II) increased in the cell culture. The saturation of the MeHg production was also observed with time of exposure to Hg for other microorganisms, such as various sulfate-reducing strains including *Pseudodesulfovibrio mercurii* ND132[13−15] and the iron-reducing strain *Geobacter sulfurreducens* PCA.[15] However, the specific limiting steps that account for the saturation of MeHg production were not identified.

Hg(II) methylation is performed in the cell cytosol, where HgcA, a putative corrinoid protein, is expected to transfer a methyl group to Hg(II). HgcA is associated with HgcB, a ferredoxin-like protein, that carries out the corrinoid reduction.[16] Accordingly, the methylation reaction in the cytosol follows the Michaelis−Menten equation[17] where methylation rates (in nM/h) reach a plateau with time due to a saturation of the enzyme catalytic sites. Before entering the

Received: October 31, 2024
Revised: January 29, 2025
Accepted: January 29, 2025

cell cytosol for methylation, Hg(II) is taken up by the cells. The Hg(II) uptake step is still not fully understood: while some studies evidenced a passive uptake,[18] others suggested an active or facilitated uptake mechanism.[19] Furthermore, it remains unknown whether the process of Hg(II) uptake exhibits saturation over time or with increasing concentrations of Hg(II). Nonetheless, the saturation in intracellular Hg(II) uptake may provide an explanation for the observed saturation in MeHg production by a sulfate-reducing strain in previous studies as Hg(II) concentrations increased.[11,12]

The net production of MeHg arises from the combined processes of Hg(II) methylation and MeHg demethylation. MeHg can be degraded either through abiotic pathways[20] or biotic pathways,[20−22] sometimes involving the same microorganisms responsible for Hg(II) methylation.[21] The saturation of MeHg production with an increasing Hg(II) concentration may be attributed to an enhanced degradation of MeHg. To elucidate the rate constant for Hg(II) methylation and the concomitant rate of MeHg demethylation, kinetic experiments can be conducted in order to fit the measured concentration of produced MeHg ($[MeHg]_t/[Hg(II)]_0$) to a reversible reaction model.[23]

Various key mechanistic studies were performed for only 1 or 2 time points.[12,24−26] In these studies, short-term or equilibrium-based events might not have been detected, although they could be critical to understanding the cascade of events. For example, nanosized $HgS_{(s)}$ has been observed around Hg methylating cells[12,24] and several authors have discussed their bioavailability and potential implications for MeHg production.[27,28] However, it is still unclear how fast these nanosized $HgS_{(s)}$ are formed and how their structure or localization changes over time. Time-resolved experiments are also needed to investigate the intracellular trafficking of Hg(II) and MeHg, at the cellular level. For example, An et al. (2019)[18] showed an increase in intracellular Hg(II) in *Pseudodesulfovibrio mercurii* ND132 over time for a Hg concentration of 0.025 μM. Conducting a time-resolved study on intracellular Hg(II) accumulation by a Hg(II) methylating bacterium at various Hg(II) concentrations would help to determine whether Hg(II) uptake exhibits saturation.

The objective of this study was to explore the limiting steps in MeHg production as the concentration of Hg(II) increases. Specifically, we aimed to determine whether the uptake of Hg(II), the intracellular methylation of Hg(II), the MeHg degradation, or the release of MeHg by the cells were the factors constraining MeHg production. For that, we performed a time-resolved experiment (0.1, 1, 4, and 24 h) with various Hg(II) concentrations (from 0.03 to 3.15 μM, with 3 to 5 different concentrations). We used the sulfate-reducing strain *Pseudodesulfovibrio hydrargyri* BerOc1 to methylate Hg(II) and demethylate MeHg. Particularly, we determined (i) the rates of methylation and demethylation, (ii) the distribution of Hg(II) and MeHg among the extracellular medium, the fraction adsorbed to the cells, and the intracellular fraction, to track the import/export of Hg(II) and MeHg during bacterial growth, as a function of Hg(II) concentration. We used gas chromatography-inductively coupled plasma mass spectrometry (GC-ICP-MS) to quantify Hg(II) and MeHg in the different fractions, and scanning transmission electron microscopy combined with energy dispersive X-ray spectroscopy (STEM-EDS) to localize Hg in or around the cells during the MeHg production.

2. MATERIALS AND METHODS

2.1. Microbial Culture Conditions. The sulfate-reducing strain *Pseudodesulfovibrio hydrargyri* BerOc1 was isolated from the sediments of the Berre Lagoon (France) and characterized in previous studies.[11,12,29,30] BerOc1 was grown in anaerobic conditions under fumarate respiration, in the dark at 37 °C in multipurpose medium (see SI part I.1 and Table S1) with pyruvate (40 mM) as a carbon source and electron donor, fumarate (40 mM) as an electron acceptor, and SO_4^{2-} (0.1 mM). At this sulfate concentration, the energy produced by the sulfate respiratory metabolism (dissimilatory sulfate reduction) is insufficient to support cell growth.[31,32] Instead, sulfate was added to serve as a sulfur source. To avoid culture heterogeneity, the medium (500 mL) was inoculated with 10% of fresh preculture and then distributed in culture tubes (7.2 mL) for Hg exposure, in an anoxic chamber (95%N_2 /5% H_2 v/v). The culture tubes were sealed with stoppers covered by a PTFE layer and incubated at 37 °C in hermetic boxes containing O_2 absorbers flushed with N_2. The growth was monitored by measuring the optical density (OD) at 600 nm with a spectrophotometer (Spectronic CamSpec Ltd. M107).

The cultures were spiked with 40 μL of Hg(II) spike solution in the anoxic chamber during the exponential growth phase (i.e., when the cell population had doubled at least once, see Figure S1A). The Hg(II) spike solutions were prepared by diluting a stock solution of $HgCl_2$ (9 mM concentration in 1% HNO_3) in anoxic, sterile deionized water. The cells were exposed to five different Hg(II) concentrations (0.03, 0.33, 0.43, 1.20, and 3.15 μM) and incubated at 37 °C in the dark for 0.1 h (i.e., 6 to 8 min), 1 h, 4 h, or 24 h in triplicates (except for concentrations 0.33 and 0.43 μM, which were tested in duplicates at time points 0.1 h and 24 h). The Hg(II) exposure concentrations were consistent with levels reported in perturbed environments such as sediment rivers in urban or mining areas.[33] An additional culture tube was prepared for each Hg(II) concentration condition to monitor microbial growth after the last sampling point, and a control with no Hg (in triplicates) was prepared to assess the impact of Hg on bacterial growth (Figure S1A and SI Part I.2.). Two types of abiotic controls were performed to quantify the abiotic Hg(II) methylation in cultures: culture medium without cells and a heat-inactivated (1 h, 80 °C) culture. For both types of controls, Hg(II) was spiked to a final concentration of 0.02−0.03, 1.36−1.64, and 3.70−3.64 μM (measured concentrations) and sampled after 24 h. At each time point, aliquots were sampled for (i) flow cytometry analysis to determine the cell number, (ii) sulfide concentration determination, and (iii) Hg(II) and MeHg partitioning among different fractions (bulk fraction, extracellular fraction, adsorbed to the cells fraction, and intracellular fraction).

For cell counting, 1.6 mL was sampled and stored at −80 °C in filtered formaldehyde (5% (v/v)). The cells were tagged with 10X SYBR (Invitrogen) for 15 min in the dark. The number of cells was determined by flow cytometry in a BD Accuri C6 cytometer (BD Biosciences) using Trucount beads (BD). Sulfide concentration was determined according to the methylene blue method[34] using a spectrophotometer at 670 nm. To predict the precipitation of metacinnabar (β-HgS) in the culture medium, we used Visual Minteq software and its equilibrium constant database (Table S2). The thermodynamic calculations were performed with the initial culture

https://doi.org/10.1021/acsearthspacechem.4c00327
ACS Earth Space Chem. XXXX, XXX, XXX−XXX

composition (Table S1) without sulfate and with the sulfide concentration measured at 0.1 h after Hg exposure.

2.2. Mercury Species (Hg(II) and MeHg) Partitioning. At the end of Hg exposure (0.1, 1, 4, or 24 h), a 0.5 mL aliquot of the cell culture was collected for the quantification of total Hg(II) and MeHg concentrations (*bulk fraction*). The remaining culture was centrifuged at 4 °C and 6000*g* for 30 min. A 0.5 mL aliquot of the supernatant was collected for Hg(II) and MeHg analysis (*extracellular fraction*). The cell pellet was subjected to a two-step desorbing procedure[35] to extract the cell-adsorbed Hg. First, the cell pellet was resuspended in 2.5 mL of the first desorbing solution (50 mM EDTA disodium salt dihydrate (>98%, Thermo Fisher Scientific), 100 mM sodium oxalate (>99.5%, Sigma-Aldrich), pH 7.5) and agitated for 10 min. Then, 2.5 mL of the second desorbing solution (10 mM reduced L-glutathione (>98%, Sigma-Aldrich), 3 mM L-ascorbate sodium salt (>99%, Thermo Fisher Scientific, pH 7) was added, and the cell suspension was agitated again for 10 min. The suspension was subsequently filtered using a syringe and a polycarbonate filter holder (Sartorius) with a 0.22 μm PVDF filter. A 0.5 mL aliquot of the filtrate was collected for the Hg(II) and MeHg analysis (*adsorbed to the cells fraction*). The cell membranes were not impacted by the desorbing procedure (SI Part II.1, Figure S3). The efficiency of the desorption procedure for removing Hg compounds from the cell membranes was evaluated, as detailed in SI Part II.2, Figure S4. All of the aliquots were immediately digested in 6 N HNO_3 (50% v/v) after sampling, to stop the reactions and extract Hg(II) and MeHg. The cells remaining on the filter after the desorbing procedure were recovered by immersing the filter in 2 mL of 6 N HNO_3 (*intracellular fraction*). The fractions were stored at 4 °C until analysis.

The proportion of Hg (Hg(II) or MeHg) in the extracellular medium (f_{extra}) was determined by dividing the mass of Hg determined in the *extracellular fraction* (mHg_{extra}) by the mass of Hg measured in the *bulk fraction* (mHg_{bulk}), as described in eq 1:

$$f_{extra} = \frac{mHg_{extra}}{mHg_{bulk}} \tag{1}$$

A recovery factor for the fractionation was calculated by adding the mass of Hg from the extracellular, adsorbed to the cells, and intracellular fractions and compared to the mass of Hg measured in the bulk fraction. The median value was 90% for MeHg (ranging from 36 to 137%) and 40% for Hg(II) (ranging from 13 to 58%). We attributed the low recovery, particularly for Hg(II), to a loss of cells during the supernatant pouring step (Figure S2). To overcome this unavoidable loss, the proportion of Hg associated with the cells (f_{cells}) was determined by subtracting the mass of Hg in the *extracellular fraction* (mHg_{extra}) from the mass of Hg in the *bulk fraction* (mHg_{bulk}), as described in eq 2:

$$f_{cells} = \frac{mHg_{bulk} - mHg_{extra}}{mHg_{bulk}} \tag{2}$$

Then, the intracellular (f_{intra}) and adsorbed to the cells ($f_{adsorbed}$) proportions were calculated from f_{cells} and the masses of Hg determined in the *intracellular fraction* (mHg_{intra}) and in the *adsorbed to the cells fraction* ($mHg_{adsorbed}$), as described in eqs 3 and 4:

$$f_{intra} = \frac{mHg_{intra}}{mHg_{intra} + mHg_{adsorbed}} \times f_{cells} \tag{3}$$

$$f_{adsorbed} = \frac{mHg_{adsorbed}}{mHg_{intra} + mHg_{adsorbed}} \times f_{cells} \tag{4}$$

The values presented are averages of three biological replicates, along with their corresponding standard deviations. The recovery of Hg after the filtration step was determined with the control tubes without cells and showed less than 10% loss on average for the three tested concentrations (Supplementary raw data file).

2.3. Hg(II) and MeHg Analysis. Hg(II) and MeHg concentrations were measured by capillary gas chromatography (GC TriPlus RSH, Thermo Scientific) connected to an inductively coupled plasma mass spectrometer (X2-series, Thermo Electron). Quantification for each Hg species concentration was performed by isotopic dilution, as previously described by Monperrus et al.[36] Briefly, known amounts of fractions (bulk, extracellular, adsorbed to the cells, and intracellular fractions) were buffered at pH 3.9 using a 0.1 M acetic acid/acetate buffer and then spiked with a known quantity of isotopically enriched Hg species (^{199}Hg(II) and Me^{201}Hg). Hg(II) and MeHg were ethylated using 5% (v/v) $NaBEt_4$ and extracted in iso-octane by shaking vigorously for 20 min. The organic phase containing Hg species was collected and analyzed by GC-ICP-MS. Each sample was measured three times. The isotopic dilution was shown to be successful in correcting for matrix effects in Hg species measurements by GC-ICP-MS.[36] Therefore, the presence of ligands (e.g., glutathione, EDTA) should not affect the measurement.

2.4. Hg Methylation and MeHg Demethylation Rate Constants Determination. The specific methylation and demethylation rate constants (K_m and K_d) can be calculated from time series experiments by using a first-order reversible reaction kinetic model. The mathematical steps in assessing the rate constants are discussed in detail by Martin-Doimeadios et al.[23] Assuming a pseudo-first-order reversible reaction, the net MeHg formation could be expressed as shown in eq 5:

$$\frac{d[\text{MeHg}]}{dt} = K_m[\text{Hg(II)}]_0 - K_d[\text{MeHg}] \tag{5}$$

By applying a nonlinear fitting model (Box Lucas1, OriginLab software), methylation and demethylation rate constants were calculated for each time series data set using the relationship defined in eq 6:

$$\frac{[\text{MeHg}]}{[\text{Hg(II)}]_0} = \frac{K_m}{K_m + K_d}(1 - e^{-(K_m+K_d)t}) \tag{6}$$

where $[\text{Hg(II)}]_0$ is the initial substrate concentration measured at the start of the assays.

Relative error on K_m (E_{Km}/K_m) was calculated based on eq 7 from the absolute errors $E_{Km/(Km+Kd)}$ and E_{Km+Kd} resulting from the fit for the parameters $\frac{K_m}{K_m + K_d}$ and $K_m + K_d$, respectively:

$$\frac{E_{Km}}{Km} = \sqrt{\left(\frac{E_{Km/Km+Kd}}{\frac{Km}{Km+Kd}}\right)^2 + \left(\frac{E_{km+kd}}{Km + Kd}\right)^2} \tag{7}$$

Absolute error on K_d (E_{Kd}) was calculated based on eq 8 from the absolute errors E_{Km+Kd} and E_{Km} on the parameters ($K_m + K_d$) and K_m:

https://doi.org/10.1021/acsearthspacechem.4c00327
ACS Earth Space Chem. XXXX, XXX, XXX−XXX

$$E_{Kd} = \sqrt{(E_{Km+Kd})^2 + (E_{Km})^2} \quad (8)$$

Relative error on K_m/K_d was calculated based on eq 9:

$$\frac{E_{Km/Kd}}{Km/Kd} = \sqrt{\left(\frac{E_{Km}}{Km}\right)^2 + \left(\frac{E_{Kd}}{Kd}\right)^2} \quad (9)$$

2.5. Scanning Transmission Electron Microscopy (STEM) Coupled with Energy Dispersive X-Ray (EDS). To follow the interactions of Hg with bacterial cells over time, cells were imaged by scanning transmission electron microscopy (STEM). Cells were obtained from a second culture of BerOc1, under the same conditions as described in the "Microbial culture conditions" section. Cells were exposed to 5 μM $HgCl_2$ during the exponential growth phase. At different time points after the Hg(II) spike (0.1, 1, 4, and 9 h), a culture tube (V = 16.5 mL) was collected: the culture was centrifuged at 6000g for 30 min at 4 °C. The supernatant was discarded, and the pellet containing the cells was washed with anoxic autoclaved ultrapure water (6000g for 30 min at 4 °C). The washed cell pellets were diluted in anoxic ultrapure water, and a drop was deposited on pins. Pins were rapidly plunged in liquid isopentane and cooled with liquid nitrogen. The samples were then cryo-sectioned to a thickness of 150 nm with a Diatome CryoImmuno diamond knife and air-dried. Cells were analyzed with the Thermo Fisher Talos F200S at the BIC (Bordeaux, France), with an accelerating voltage of 200 kV. Images were acquired in STEM mode, with a high angle annular dark field (HAADF) and energy dispersive X-ray (EDS) detectors, aided by the Thermo Fisher Velox software.

3. RESULTS AND DISCUSSION

3.1. Kinetic Analysis of Simultaneous Methylation and Demethylation. The cultures were supplemented with Hg(II) during the exponential growth phase, precisely 14 h after initiating the growth of the cultures. Based on biomass production and sulfide consumption (Figure S1B,C), the addition of Hg(II) during exponential growth exhibited no impact on bacterial growth regardless of Hg(II) concentration. However, the extents and kinetic rates of Hg(II) transformation into MeHg processed by BerOc1 varied, depending on the initial Hg(II) concentration (Figure 1 and Table S4) and cannot be explained by abiotic transformations (Table S4).

First, a saturation of MeHg production with time was observed for the lowest concentration (0.03 μM): there was a fast MeHg production during the first hours of exposure, followed by a plateau reached after approximately 4 h of Hg(II) exposure (Figure 1 and Table S4). At higher concentrations, a plateau was less clearly observed, even after 24 h of incubation (Figure 1) but MeHg production was not linear, suggesting that MeHg production was also getting slower with time, except for the highest concentration (3.15 μM).

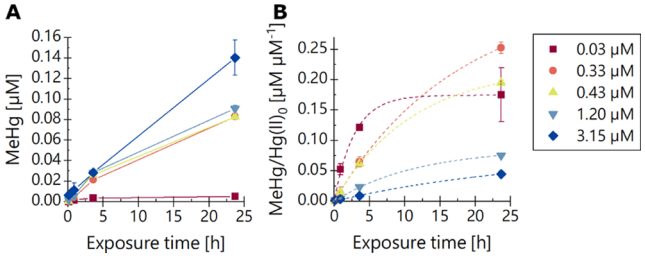

Figure 1. (A) MeHg production in μM and (B) MeHg production normalized by the initial Hg(II) concentration ($[Hg(II)]_0$), over time, for the five tested concentrations (0.03, 0.33, 0.43, 1.20, and 3.15 μM). The values and error bars are averages and standard deviations for the two or three replicates. The dashed curves in (B) show the fit obtained by the first-order reversible reaction model.

With an increasing Hg(II) concentration, MeHg production increased (Figure 1A). However, the production normalized by the initial Hg(II) concentration tended to decrease with an increasing concentration (Figure 1B), suggesting a saturation of the methylation process with an increasing concentration. Second, the Hg(II) methylation potential (i.e, [MeHg]/$[Hg(II)]_0$ at the end of the growth phase) increased from an initial concentration of 0.03 to 0.33 μM (17.2 to 25.2%) and then decreased from 0.43 μM to 3.15 μM (25.2 to 4.5%) (Figure 2A). These findings are consistent with those of previous research. For instance, an increase in methylation potential was observed over the Hg(II) concentration range from 0.005 μM to 0.125 μM with the iron-reducing bacterium *Geobacter bemidjiensis* Bem.[22] Additionally, a decrease in methylation potential at higher concentrations was noted, such as within 0.005 to 500 μM of Hg(II) with the SRB *P. mercurii* ND132[37] or with BerOc1, within a range of 0.05 to 5 μM, suggesting a saturation of the MeHg production with increasing Hg(II) concentration.[11,12] Here, the additional Hg(II) concentrations tested (0.33 and 1.2 μM) evidenced a nonlinear relationship, as there was a higher methylation potential observed for the intermediate concentrations (0.33 and 0.43 μM).

To gain a deeper understanding of the saturation of MeHg production with time (at 0.03 μM) and with Hg(II) concentration, it was essential to decouple Hg(II) methylation and MeHg demethylation rates from the net reaction. Indeed, MeHg demethylation was already observed for the strain BerOc1.[12] For that, MeHg production was fitted with a pseudo-first-order reversible reaction model, enabling the determination of both the Hg(II) methylation rate (K_m) and the MeHg demethylation rate (K_d). The values obtained for K_m (ranging from 0.003 ± 0.002 h^{-1} to 0.061 ± 0.013 h^{-1}) and K_d (ranging from 0.033 ± 0.021 h^{-1} to 0.290 ± 0.072 h^{-1}) were approximately one order of magnitude higher compared to *Desulfobulbus propionicus* DSM6523[21] and other experiments on *P. hydrargyri* BerOc1[38] (Table S5). These variations could be attributed to strain specificities and/or to differences in culture conditions (e.g., lower electron donor/acceptor concentration in the study by Perrot et al.).[38] The K_m values decreased with increasing Hg(II) concentration (Figure 2B), whereas K_d remained stable, except for the lowest concentration (Figure 2B). Finally, when plotting the K_m/K_d ratio (representing net MeHg production) against initial Hg(II) concentrations, the trend suggests a bell shape (Figure 2C), as observed for the Hg(II) methylation potential (Figure 2A).

The successful fitting results for all five concentrations suggest that MeHg production follows a reversible reaction (Figure 1B). The observed plateau in MeHg production at the lowest concentration (0.03 μM) can be attributed to a high demethylation rate (0.290 h^{-1}). K_m decreased with increasing Hg(II) concentration, indicating the saturation of the methylation process, independently of a concomitant decrease in the demethylation process. Although the highest K_m value (0.061 h^{-1}) was observed at 0.03 μM, the measured methylation potential was not the highest (17.5% of initial

https://doi.org/10.1021/acsearthspacechem.4c00327
ACS Earth Space Chem. XXXX, XXX, XXX−XXX

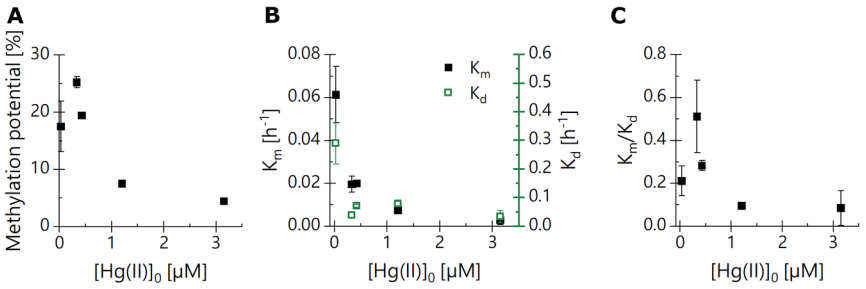

Figure 2. (A) Hg(II) methylation potential ($[MeHg]/[Hg(II)]_0 \times 100$) after 24 h of exposure. The values and error bars are averages and standard deviations for the two or three replicates. (B) Hg(II) methylation rate K_m (black squares) and MeHg demethylation rate K_d (green empty squares) depending on the initial Hg(II) concentration ($[Hg(II)]_0$); error bars are calculated from errors on fit parameters (see Materials and methods section). (C) K_m/K_d ratio depending on the initial Hg(II) concentration; error bars are calculated from errors on fit parameters (see Materials and methods section).

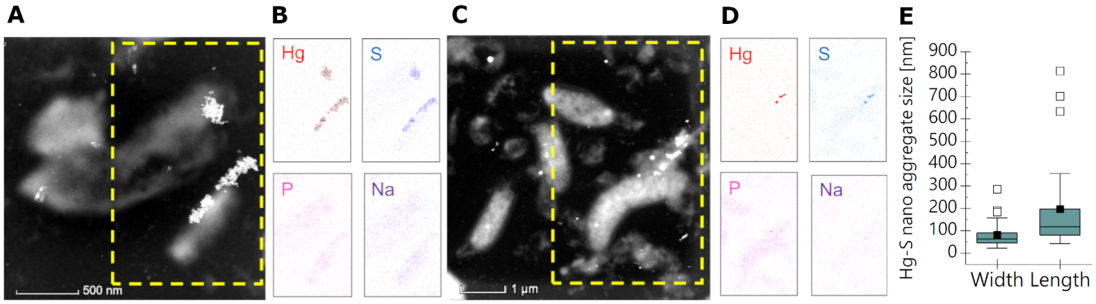

Figure 3. STEM images of BerOc1 cells after (A, B) 0.1 h and (C, D) 9 h of exposure to 5 μM of Hg(II). (A) and (C) show HAADF images and (B) and (D) show EDS elemental maps in the yellow dashed lined zone defined in HAADF images. (E) Size distribution of the Hg-S aggregates observed (two dimensions are plotted: length and width; n = 35 from 14 images, see SI Part VI).

Hg), due to the highest K_d value (0.290 h^{-1}) at this concentration. Between 0.03 and 0.33 μM Hg, the decrease in K_d was greater than the decrease of K_m, explaining the highest methylation potential observed at the 0.33 μM Hg concentration.

The results evidenced a saturation of the methylation process, as evidenced by decreasing K_m values with an increasing Hg(II) concentration. However, the model we used does not account for Hg(II) availability and cellular uptake. In the next sections, our focus will shift toward determining the temporal dynamics of Hg(II) and MeHg, particularly within distinct cellular fractions. Our specific goal was to investigate Hg(II) uptake and MeHg export processes in relation to varying Hg(II) concentrations.

3.2. Rapid Formation of Hg-S Nanoparticles. To investigate Hg accumulation within the bacterial cells, we first characterized the HgS precipitates formed during bacterial growth.[12,24,39] Thermodynamic calculations, based on the initial composition of the culture medium (Table S1) and the sulfide concentration measured 0.1 h after the Hg spike (Figure S1C), showed that more than 99.9% of the Hg(II) would precipitate as $HgS_{(s)}$, either as cinnabar (α-HgS) or metacinnabar (β-HgS) for all Hg(II) concentrations tested (Table S3). While these theoretical calculations have some limitations (e.g., not considering changes in the culture medium and produced thiols), the stability constants suggest that the formation of $HgS_{(s)}$ is likely to occur during the experimental assays. Therefore, we investigated the temporal formation, size, and localization of these $HgS_{(s)}$ complexes using STEM imaging.

The cells exposed to 5 μM of Hg(II) were imaged by STEM at 0.1 and 9 h after the Hg(II) spike (Figure 3). It was previously shown that 5 μM of Hg(II) does not impact BerOc1 growth.[11,12] Hg was observed outside the cells, close to the membranes, colocalized with sulfur and occasionally with other elements (Zn, P, and Mg) (Figures 3B,D and S5−S7). The Hg and S-containing particles (Hg-S nanoparticles) had a size of approximately 5 nm and formed aggregates with a median size of 66 nm in width and 126 nm in length, as observed in 35 aggregates observed in 14 images (Figures 3E and S5 − S7). Similar aggregates were also previously imaged outside of the cells by Isaure et al.[12] with the same bacterial strain with a lower initial sulfate concentration (4 μM versus approximately 100 μM in this study). Thermodynamic calculations indicated the formation of metacinnabar (β-HgS) or cinnabar (α-HgS) (Table S3), but the β-HgS form is more likely as it has been previously identified in cultures of cells grown in anaerobiosis, including BerOc1.[12] Nanosized β-$HgS_{(s)}$ particles were also observed with electron microscopy around other nonsulfate-reducing strains, i.e., *Escherichia coli* ATCC 25922 and *Geobacter sulfurreducens* PCA[24] under different growth conditions. We could also expect the formation of extracellular nanosized $HgS_{(s)}$ even with less sulfide as compared to our study (S^{2-}:Hg molar ratio of ~30), as $HgS_{(s)}$ may also form from Hg−thiolates complexes.[40] Our observation, together with previous studies,[12,24] suggests a ubiquitous formation of extracellular β-$HgS_{(s)}$ nanoparticles in the presence of Hg in anoxic bacterial cultures, despite different culture media.

Notably, the particles were observed as soon as 0.1 h after the Hg addition in the medium (Figure 3A, B), showing a fast formation of these nanosized compounds. The early precipitation of $HgS_{(s)}$ could have implications for Hg(II) uptake and methylation by BerOc1. Indeed, previous studies showed MeHg produced from nanosized $HgS_{(s)}$.[14,27,28,41]

https://doi.org/10.1021/acsearthspacechem.4c00327
ACS Earth Space Chem. XXXX, XXX, XXX−XXX

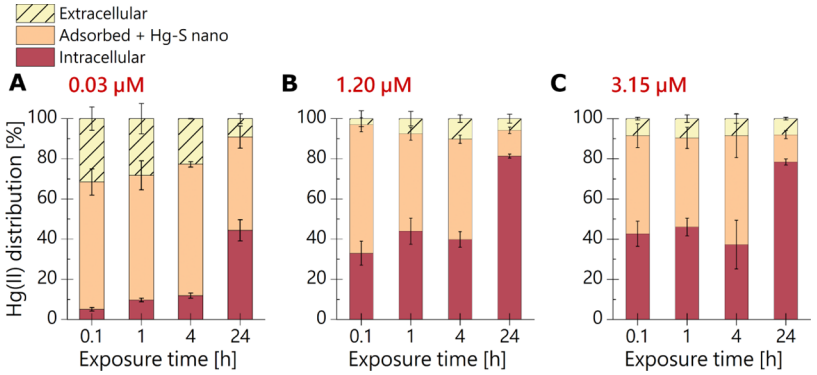

Figure 4. Hg(II) distribution among three fractions (intracellular; adsorbed-to-the cells + Hg−S nanoparticles; extracellular) for the three tested Hg(II) concentrations (A) 0.03 μM, (B) 1.20 μM, and (C) 3.15 μM and for the four time points (0.1, 1, 4, and 24 h). The values and error bars are the averages and standard deviations for the three replicates. (Note: Hg(II) here refers exclusively to inorganic divalent Hg and does not include MeHg.)

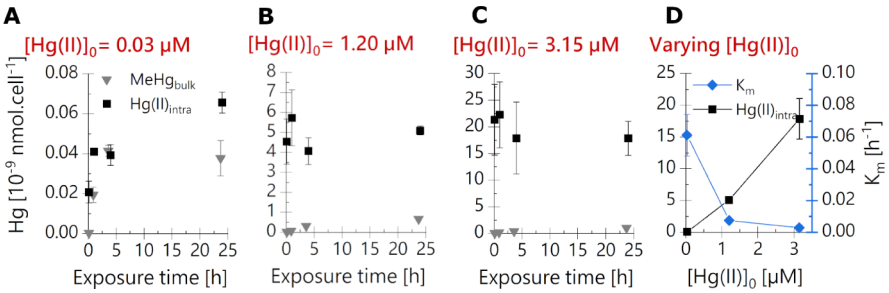

Figure 5. Intracellular Hg(II) (black squares) and MeHg produced (MeHg measured in the bulk fraction, gray triangles) normalized by the number of cells for an initial Hg(II) concentration of (A) 0.03 μM, (B) 1.20 μM, (C) 3.15 μM, over time. (D) Intracellular Hg(II) after 24 h of incubation as a function of the Hg(II) initial concentration, compared with the K_m trend (blue diamonds). The values and error bars are averages and standard deviations for the three replicates.

However, it is not clear whether the nanosized $HgS_{(s)}$ is directly taken up by the cells, or if the cells uptake Hg(II) released by $HgS_{(s)}$ dissolution.[27] In this study, Hg was mostly observed outside of the cells with STEM, (even if in several regions of the images no clear distinction could be made between intra- or extracellular Hg (Figure 3A top cell, Figures S6B and S7B)), suggesting that Hg is highly diluted and not present as aggregated Hg-S nanoparticles inside the cell. This implies that the uptake of Hg is likely to occur as dissolved Hg(II), Hg(II) bound to organic molecules, or potentially highly dispersed $HgS_{(s)}$. Previous studies have evidenced an enhanced Hg(II) methylation with sulfidized organic matter[42] or hydrophobic natural organic matter.[43] This could be a result of ligand-facilitated $HgS_{(s)}$ dissolution[44] or limitation of $HgS_{(s)}$ growth and aggregation by organic molecules,[45−47] which would increase Hg(II) availability and uptake by Hg(II) methylators and, in turn, Hg(II) methylation. Indeed, we expect thiols to be produced based on other studies with BerOc1 (0.150 μM)[48] or with *Geobacter sulfurreducens* (0.120 μM).[49] In this study, a change of aggregate size over the 9 h of Hg(II) exposure was not observed (Figure S8), likely because the aging effects previously observed by Pham et al.[27] at the atomic scale and responsible for a lower methylation potential are not observable with STEM.[27]

3.3. Accumulation of Hg(II) in the Cells. To investigate Hg(II) accumulation in the cells, we analyzed three cellular fractions: the extracellular fraction, the adsorbed-to-the-cells fraction, and the intracellular fraction. The adsorbed-to-the-cells fraction includes previously identified Hg-S nanoparticles (approximate size of 5 nm). Indeed, we observed that the desorbing procedure efficiently removed Hg-S nanoparticles adsorbed to the cell membranes (see SI part II.2, Figure S4). Consequently, the fraction was renamed "adsorbed + Hg-S nano". In this fractionation experiment, we specifically focused on (i) the lowest concentration (0.03 μM), which exhibited the highest methylation rate (K_m = 0.061 h^{-1}), (ii) the highest concentration (3.15 μM) showing the lowest methylation rate (K_m = 0.003 h^{-1}) and an intermediate Hg(II) concentration (1.20 μM, K_m = 0.007 h^{-1}) (Figure 2B). For each concentration and time point, Hg(II) was mostly (68−94%) associated with the cells ("adsorbed + Hg-S nano" and "intracellular") (Figure 4), in agreement with previous studies.[11−13,26] This could be attributed to the presence of precipitated $HgS_{(s)}$ in this fraction obtained either by centrifugation[11,12,26] or filtration at 0.22 μm.[13] However, to determine whether Hg(II) uptake is a saturating process, it was necessary to discriminate intracellular Hg(II) from adsorbed Hg(II) and extracellular $HgS_{(s)}$. To achieve this, we desorbed the Hg adsorbed to the cells using a washing procedure followed by filtration at 0.22 μm.

Hg(II) uptake dynamics followed a different pattern depending on the Hg(II) concentration (Figures 4 and 5). At the lowest concentration (0.03 μM), an increase in intracellular Hg(II) was measured and was concomitant with a decrease in extracellular Hg(II) over time (Figure 4A). Moreover, at this concentration, less than 12% of Hg(II) was intracellular during the first 4 h (Figure 4A) although the methylation process was close to reaching saturation (Figure 1). While the net MeHg production per cell was slowing down due to the concomitant MeHg degradation between 4 and 24 h

https://doi.org/10.1021/acsearthspacechem.4c00327
ACS Earth Space Chem. XXXX, XXX, XXX−XXX

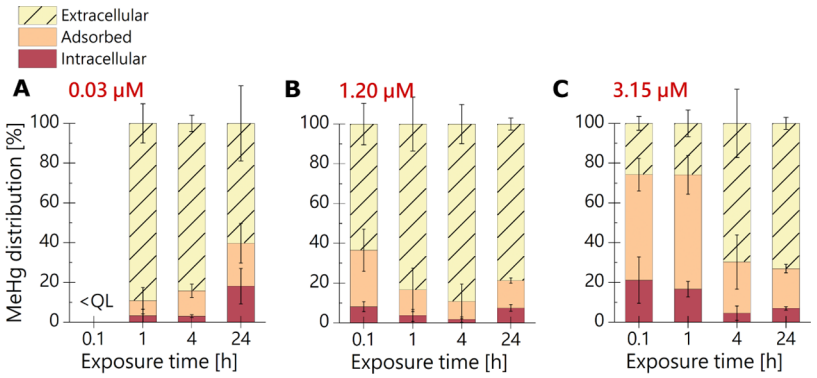

Figure 6. MeHg distribution among the three fractions (intracellular, adsorbed to the cells, and extracellular) for the three tested Hg(II) concentrations (A) 0.03, (B) 1.20, and (C) 3.15 μM measured at four time points (0.1, 1, 4, and 24 h). The distribution of MeHg at 0.1 h of exposure at 0.03 μM was not shown because the concentration was below quantification limit (QL, i.e., $<5\times10^{-4}$ μM). The values and error bars are averages and standard deviations for the three replicates.

(Figure 1), the intracellular Hg(II) pool increased (Figures 4A and 5A). This result suggests that Hg(II) accumulated by the cells between 4 and 24 h of exposure was not methylated, or was methylated and quickly demethylated, leading to an increase of intracellular Hg(II). This result corroborates previous studies showing an increase of intracellular Hg(II) for *Pseudodesulfovibrio mercurii* ND132 within 10 or 24 h in active cells[18,50] or heat-killed and starved cells[18] at low Hg(II) concentration (0.025 μM). At higher concentrations, however, an equilibrium between intracellular Hg(II) concentration and extracellular Hg(II) concentration was already reached after 0.1 h of Hg(II) exposure (Figure 4B,C). The amount of intracellular Hg(II) per cell did not increase over time (Figure 5B,C) and the increase in the proportion of intracellular Hg(II) observed in % (Figure 4B,C) simply reflected the increasing number of cells over time (Figure S1A,B).

Interestingly, the amount of Hg(II) in the cells after 24 h increased linearly with increasing initial Hg(II) concentration (Figure 5D). This result was also verified at each time point (data not shown) and indicates that Hg(II) intracellular accumulation was not saturating between 0.03 and 3.15 μM: the more Hg(II) is added to the culture, the more Hg(II) is accumulated by the cells. The observed intracellular Hg(II) accumulation could be due to increased Hg(II) uptake and/or limited Hg(II) export. Increasing Hg(II) concentration in the extracellular medium could increase Hg(II) uptake in order to reach an equilibrium between the intracellular and extracellular medium. This would be in line with the passive uptake suggested by Benoit et al.[51,52] and An et al.[18] Regarding limiting Hg(II) export, if the Hg(II) methylation process is saturating, then the bacterium could use a parallel Hg detoxification process involving precipitation with thiols or $HgS_{(s)}$ precipitation, which would be less easily exported from the cell. Liu et al.[50] already suggested this hypothesis for *Pseudodesulfovibrio mercurii* ND132. As an example, glutathione was recently identified as an intracellular ligand of Hg(II) in a cyanobacterium cell.[53] It remains necessary to investigate intracellular Hg(II) speciation and environmental parameters controlling Hg(II) accumulation in the cells.

The rise of intracellular Hg(II) levels in response to an increasing extracellular Hg(II) pool (Figure 5D) was not concurrent with an augmentation in Hg(II) methylation potential (Figure 2A) or methylation rates (Figure 5D). These findings indicate that intracellular Hg(II) may not be the limiting factor influencing Hg(II) methylation. Moreover, the plateau observed at 0.03 μM for the produced MeHg (Figures 1 and 5A) was not explained by limited Hg(II) uptake, as intracellular Hg(II) was still increasing (Figure 5A). These results question the fate of intracellular Hg(II), if not methylated. An et al.[18] showed that a significant part of the intracellular Hg(II) was adsorbed on the cytoplasmic membrane of *P. mercurii* ND132. The authors proposed that the Hg(II) pool adsorbed on the cytoplasmic membrane is the one available for the transmembrane HgcA protein, whereas the internalized Hg(II) is not available.[18] Wang et al.[54] also suggested that *Geobacter sulfurreducens* PCA produces MeHg independently of the accumulation of intracellular Hg(II) within the periplasm and cytosol. Additionally, Gutensohn et al.[55] observed that the complexation of Hg(II) with cysteine as $Hg(cys)_2$ in the medium shifted the partitioning of Hg(II) from the cells to the dissolved phase, thereby increasing Hg(II) bioavailability and methylation by *G. sulfurreducens*. Intracellular but not methylated Hg(II) needs to be further investigated, as it may reduce the bioavailability of Hg(II) to Hg(II) methylators as well as toxicity to other organisms.

3.4. Dynamics of MeHg Export. The distribution of MeHg (Figure 6) shows that MeHg was mostly extracellular for all three concentrations (60−90%), except for the early time points at the highest concentration (<26%). MeHg distribution among cellular fractions can vary depending on the strain (e.g., sulfate-reducing bacteria, iron-reducing bacteria, or methanotrophs)[56] or the medium composition (e.g., presence of thiols).[25] Here, the observation of extracellular MeHg aligns with previous studies investigating Hg(II) methylation by sulfate-reducing bacteria,[11−13,26,50,56] as well as iron-reducing bacteria in the presence of thiols,[19,25,57] suggesting an export of MeHg from the cell.

Furthermore, our results confirm the rapid release in the extracellular medium of the produced MeHg at low Hg(II) concentration exposure (as shown previously by Graham et al. at Hg(II) < 1 μM),[13] while indicating a slower release at high concentrations (3.15 μM). This slower release may involve a two-step process as suggested by Lin et al., which includes export by the cell and subsequent adsorption/desorption from the outer cell membrane.[25] Indeed, the adsorption of MeHg on the cells is consistent with the strong affinity of Hg(II) and MeHg for thiols,[58] the abundance of thiol functional groups in the cell membrane[59,60] and the identification of MeHg−cysteine associated with the cells.[12] The desorption of MeHg is likely to be influenced by the chemistry of the surrounding

https://doi.org/10.1021/acsearthspacechem.4c00327
ACS Earth Space Chem. XXXX, XXX, XXX−XXX

medium, particularly, the presence of residual thiols or other ligands capable of desorbing MeHg from the membrane. For example, the presence of sulfides (formed through sulfate reduction or cysteine degradation) in the extracellular medium has been shown to enhance MeHg release into the extracellular medium.[11] However, the mechanism underlying the slower desorption of MeHg at 3.15 μM is not yet fully understood and may be explained by the higher MeHg concentration. It could also involve a slower release of thiols by the cells, which would compete with the S-containing sites of the membrane for MeHg adsorption. Indeed, the ability of *P. hydrargyri* to produce and export thiols was recently evidenced.[48]

4. CONCLUSION

In conclusion, this study explored the cellular dynamics of Hg(II) and MeHg at increasing concentrations and revealed concentration-dependent mechanisms underlying the net MeHg production. The results are relevant to a range of concentrations found in perturbed environments such as urban, mining, industrial, and agricultural areas.[33] First, we evidenced the early formation of Hg-S nanoparticles of approximately 5 nm aggregated outside the cells. It remains unclear whether these particles are taken up by cells in a highly dispersed form or dissolve, allowing cells to more easily take up Hg(II) as dissolved Hg(II) or as Hg(II) bound to organic compounds. The uptake of Hg(II) by the cells increased with the Hg(II) concentration rising from 0.03 to 3.15 μM. However, the subsequent methylation of Hg(II) that occurred in the cells was saturated, most likely due to the saturation of the enzymatic sites and/or to the immobilization of intracellular Hg(II). This suggests that a part of Hg(II) accumulated in the cells was not methylated, and the fate of this accumulated intracellular Hg(II) requires further investigation, for example, by studying the speciation of intracellular Hg(II). However, it remains challenging to distinguish between intracellular Hg(II) available for methylation, Hg(II) as a product of MeHg demethylation, and Hg(II) that would be accumulated and not methylated. Finally, MeHg export was also affected by the initial Hg(II) concentration, with a fast (0.1−1 h) export to the extracellular medium for the lowest concentrations (0.03 and 1.2 μM), and a slower (1−4 h) release at the highest concentration (3.15 μM).

■ ASSOCIATED CONTENT

Supporting Information

The Supporting Information is available free of charge at https://pubs.acs.org/doi/10.1021/acsearthspacechem.4c00327.

Raw data (XLSX)

Additional information on the microbial culture conditions, microbial growth (optical density, cell numbers), sulfide and methylmercury concentrations, graphical description of the desorbing procedure, validation of the desorbing procedure (cell integrity, Hg desorption), methylation and demethylation rates from the literature, thermodynamics calculations, additional STEM images, and Hg-S aggregates size estimation (PDF)

■ AUTHOR INFORMATION

Corresponding Authors

Maureen Le Bars − *Université de Pau Et Des Pays de L'Adour, E2S UPPA, CNRS, IPREM UMR 5254, 64000 Pau, France;* Present Address: Soil Chemistry Group, Institute of Biogeochemistry and Pollutant Dynamics, Department of Environmental Systems Science, ETH Zurich, Universitätstrasse 16, CHN, CH-8092 Zurich, Switzerland; orcid.org/0000-0003-4149-4951; Email: maureen.lebars@usys.ethz.ch

Marie-Pierre Isaure − *Université de Pau Et Des Pays de L'Adour, E2S UPPA, CNRS, IPREM UMR 5254, 64000 Pau, France;* orcid.org/0000-0002-6557-5759; Email: marie-pierre.isaure@univ-pau.fr

Authors

Mathilde Monperrus − *Université de Pau Et Des Pays de L'Adour, E2S UPPA, CNRS, IPREM UMR 5254, 64600 Anglet, France;* orcid.org/0000-0002-6337-1672

Sophie Barrouilhet − *Université de Pau Et Des Pays de L'Adour, E2S UPPA, CNRS, IPREM UMR 5254, 64000 Pau, France*

Melina Petrel − *Bordeaux Imaging Center, Univ. Bordeaux, CNRS, INSERM, BIC, UAR 3420, F-33600 Pessac, France*

Marisol Goñi-Urriza − *Université de Pau Et Des Pays de L'Adour, E2S UPPA, CNRS, IPREM UMR 5254, 64000 Pau, France*

Complete contact information is available at: https://pubs.acs.org/10.1021/acsearthspacechem.4c00327

Notes

The authors declare no competing financial interest.

■ ACKNOWLEDGMENTS

We thank Emmanuel Tessier (IPREM) for his help in collecting GC-ICP-MS data. This research was supported by the E2S-UPPA New Challenge project GO-BEAM. We also acknowledge the Bordeaux Imaging Center (Bordeaux, France) and the France BioImaging infrastructure supported by the French National Research Agency (ANR-10-INSB-04, "Investments for the Future").

■ REFERENCES

(1) Gilmour, C. C.; Podar, M.; Bullock, A. L.; Graham, A. M.; Brown, S. D.; Somenahally, A. C.; Johs, A.; Hurt, R. A.; Bailey, K. L.; Elias, D. A. Mercury Methylation by Novel Microorganisms from New Environments. *Environ. Sci. Technol.* **2013**, *47* (20), 11810−11820.

(2) Podar, M.; Gilmour, C. C.; Brandt, C. C.; Soren, A.; Brown, S. D.; Crable, B. R.; Palumbo, A. V.; Somenahally, A. C.; Elias, D. A. Global prevalence and distribution of genes and microorganisms involved in mercury methylation. *Sci. Adv.* **2015**, *1* (9), No. e1500675.

(3) Compeau, G. C.; Bartha, R. Sulfate-Reducing Bacteria - Principal Methylators of Mercury in Anoxic Estuarine Sediment. *Appl. Environ. Microbiol.* **1985**, *50* (2), 498−502.

(4) Jones, D. S.; Walker, G. M.; Johnson, N. W.; Mitchell, C. P. J.; Wasik, J. K. C.; Bailey, J. Molecular evidence for novel mercury methylating microorganisms in sulfate-impacted lakes. *Isme J.* **2019**, *13* (7), 1659−1675.

(5) Vigneron, A.; Cruaud, P.; Aubé, J.; Guyoneaud, R.; Goñi-Urriza, M. Transcriptomic evidence for versatile metabolic activities of mercury cycling microorganisms in brackish microbial mats. *Npj Biofilms Microbi.* **2021**, *7* (1), 83.

(6) Capo, E.; Broman, E.; Bonaglia, S.; Bravo, A. G.; Bertilsson, S.; Soerensen, A. L.; Pinhassi, J.; Lundin, D.; Buck, M.; Hall, P. O. J.; Nascimento, F. J. A.; Björn, E. Oxygen-deficient water zones in the Baltic Sea promote uncharacterized Hg methylating microorganisms in underlying sediments. *Limnol. Oceanogr.* **2022**, *67* (1), 135−146.
(7) Gionfriddo, C. M.; Tate, M. T.; Wick, R. R.; Schultz, M. B.; Zemla, A.; Thelen, M. P.; Schofield, R.; Krabbenhoft, D. P.; Holt, K. E.; Moreau, J. W. Microbial mercury methylation in Antarctic sea ice. *Nat. Microbiol.* **2016**, *1* (10), 16127.
(8) Kidd, K.; Clayden, M.; Jardine, T.Bioaccumulation and Biomagnification of Mercury through Food Webs. In *Environmental Chemistry and Toxicology of Mercury*. Eds., Liu, G., Cai, Y., O'Driscoll, N.; John Wiley & Sons, Inc.: Hoboken, NJ, 2012; pp 455−500
(9) Lavoie, R. A.; Bouffard, A.; Maranger, R.; Amyot, M. Mercury transport and human exposure from global marine fisheries. *Sci. Rep.* **2018**, *8*, 6705.
(10) Feng, X. B.; Li, P.; Qiu, G. L.; Wang, S.; Li, G. H.; Shang, L. H.; Meng, B.; Jiang, H. M.; Bai, W. Y.; Li, Z. G.; Fu, X. W. Human exposure to methylmercury through rice intake in mercury mining areas, Guizhou province, China. *Environ. Sci. Technol.* **2008**, *42* (1), 326−332.
(11) Barrouilhet, S.; Monperrus, M.; Tessier, E.; Khalfaoui-Hassani, B.; Guyoneaud, R.; Isaure, M. P.; Goñi-Urriza, M. Effect of exogenous and endogenous sulfide on the production and the export of methylmercury by sulfate-reducing bacteria. *Environ. Sci. Pollut. Res.* **2023**, *30* (2), 3835−3846.
(12) Isaure, M. P.; Albertelli, M.; Kieffer, I.; Tucoulou, R.; Petrel, M.; Gontier, E.; Tessier, E.; Monperrus, M.; Goñi-Urriza, M. Relationship Between Hg Speciation and Hg Methylation/Demethylation Processes in the Sulfate-Reducing Bacterium *Pseudodesulfovibrio hydrargyri*: Evidences From HERFD-XANES and Nano-XRF. *Front. Microbiol.* **2020**, *11*, 584715.
(13) Graham, A. M.; Bullock, A. L.; Maizel, A. C.; Elias, D. A.; Gilmour, C. C. Detailed Assessment of the Kinetics of Hg-Cell Association, Hg Methylation, and Methylmercury Degradation in Several Desulfovibrio Species. *Appl. Environ. Microbiol.* **2012**, *78* (20), 7337−7346.
(14) Zhang, T.; Kim, B.; Leyard, C.; Reinsch, B. C.; Lowry, G. V.; Deshusses, M. A.; Hsu-Kim, H. Methylation of Mercury by Bacteria Exposed to Dissolved, Nanoparticulate, and Microparticulate Mercuric Sulfides. *Environ. Sci. Technol.* **2012**, *46* (13), 6950−6958.
(15) Janssen, S. E.; Schaefer, J. K.; Barkay, T.; Reinfelder, J. R. Fractionation of Mercury Stable Isotopes during Microbial Methylmercury Production by Iron- and Sulfate-Reducing Bacteria. *Environ. Sci. Technol.* **2016**, *50* (15), 8077−8083.
(16) Parks, J. M.; Johs, A.; Podar, M.; Bridou, R.; Hurt, R. A.; Smith, S. D.; Tomanicek, S. J.; Qian, Y.; Brown, S. D.; Brandt, C. C.; Palumbo, A. V.; Smith, J. C.; Wall, J. D.; Elias, D. A.; Liang, L. Y. The Genetic Basis for Bacterial Mercury Methylation. *Science* **2013**, *339* (6125), 1332−1335.
(17) Date, S. S.; Parks, J. M.; Rush, K. W.; Wall, J. D.; Ragsdale, S. W.; Johs, A. Kinetics of Enzymatic Mercury Methylation at Nanomolar Concentrations Catalyzed by HgcAB. *Appl. Environ. Microbiol.* **2019**, *85* (13), No. e00438−19.
(18) An, J.; Zhang, L. J.; Lu, X.; Pelletier, D. A.; Pierce, E. M.; Johs, A.; Parks, J. M.; Gu, B. H. Mercury Uptake by *Desulfovibrio desulfuricans* ND132: Passive or Active? *Environ. Sci. Technol.* **2019**, *53* (11), 6264−6272.
(19) Schaefer, J. K.; Rocks, S. S.; Zheng, W.; Liang, L. Y.; Gu, B. H.; Morel, F. M. M. Active transport, substrate specificity, and methylation of Hg(II) in anaerobic bacteria. *Proc. Natl. Acad. Sci.* **2011**, *108* (21), 8714−8719.
(20) Barkay, T.; Gu, B. Demethylation—The Other Side of the Mercury Methylation Coin: A Critical Review. *ACS Environ. Au.* **2021**, *2* (2), 77−97.
(21) Bridou, R.; Monperrus, M.; Gonzalez, P. R.; Guyoneaud, R.; Amouroux, D. Simultaneous Determination of Mercury Methylation and Demethylation Capacities of Various Sulfate-Reducing Bacteria Using Species-Specific Isotopic Tracers. *Environ. Toxicol. Chem.* **2011**, *30* (2), 337−344.
(22) Lu, X.; Liu, Y. R.; Johs, A.; Zhao, L. D.; Wang, T. S.; Yang, Z. M.; Lin, H.; Elias, D. A.; Pierce, E. M.; Liang, L. Y.; Barkay, T.; Gu, B. H. Anaerobic Mercury Methylation and Demethylation by *Geobacter bemidjiensis* Bem. *Environ. Sci. Technol.* **2016**, *50* (8), 4366−4373.
(23) Martin-Doimeadios, R.; Tessier, E.; Amouroux, D.; Guyoneaud, R.; Duran, R.; Caumette, P.; Donard, O. F. X. Mercury methylation/demethylation and volatilization pathways in estuarine sediment slurries using species-specific enriched stable isotopes. *Mar. Chem.* **2004**, *90* (1−4), 107−123.
(24) Thomas, S. A.; Rodby, K. E.; Roth, E. W.; Wu, J. S.; Gaillard, J. F. Spectroscopic and Microscopic Evidence of Biomediated HgS Species Formation from Hg(II) - Cysteine Complexes: Implications for Hg(II) Bioavailability. *Environ. Sci. Technol.* **2018**, *52* (17), 10030−10039.
(25) Lin, H.; Lu, X.; Liang, L. Y.; Gu, B. H. Thiol-Facilitated Cell Export and Desorption of Methylmercury by Anaerobic Bacteria. *Environ. Sci. Technol. Lett.* **2015**, *2* (10), 292−296.
(26) Pedrero, Z.; Bridou, R.; Mounicou, S.; Guyoneaud, R.; Monperrus, M.; Amouroux, D. Transformation, Localization, and Biomolecular Binding of Hg Species at Subcellular Level in Methylating and Nonmethylating Sulfate-Reducing Bacteria. *Environ. Sci. Technol.* **2012**, *46* (21), 11744−11751.
(27) Pham, A. L.-T.; Morris, A.; Zhang, T.; Ticknor, J.; Levard, C.; Hsu-Kim, H. Precipitation of nanoscale mercuric sulfides in the presence of natural organic matter: Structural properties, aggregation, and biotransformation. *Geochim. Cosmochim. Acta.* **2014**, *133*, 204−215.
(28) Tian, L.; Guan, W. Y.; Ji, Y. Y.; He, X.; Chen, W.; Alvarez, P. J. J.; Zhang, T. Microbial methylation potential of mercury sulfide particles dictated by surface structure. *Nat. Geosci.* **2021**, *14* (6), 409−416.
(29) Goñi-Urriza, M.; Corsellis, Y.; Lanceleur, L.; Tessier, E.; Gury, J.; Monperrus, M.; Guyoneaud, R. Relationships between bacterial energetic metabolism, mercury methylation potential, and hgcA/hgcB gene expression in *Desulfovibrio dechloroacetivorans* BerOc1. *Environ. Sci. Pollut. Res.* **2015**, *22* (18), 13764−13771.
(30) Ranchou-Peyruse, M.; Goñi-Urriza, M.; Guignard, M.; Goas, M.; Ranchou-Peyruse, A.; Guyoneaud, R. *Pseudodesulfovibrio hydrargyri* sp nov., a mercury-methylating bacterium isolated from a brackish sediment. *Int. J. Syst. Evol. Microbiol.* **2018**, *68* (5), 1461−1466.
(31) Keller, K. L.; Wall, J. D. Genetics and molecular biology of the electron flow for sulfate respiration in. *Front. Microbiol.* **2011**, *2*, 135.
(32) Scuvée, D.; Goñi-Urriza, M.; Tessier, E.; Gassie, C.; Ranchou-Peyruse, M.; Amouroux, D.; Guyoneaud, R.; Khalfaoui-Hassani, B. Molybdate inhibits mercury methylation capacity of *Pseudodesulfovibrio hydrargyri* BerOc1 regardless of the growth metabolism. *Environ. Sci. Pollution Res.* **2024**, *31* (30), 42686−42697.
(33) Hsu-Kim, H.; Eckley, C. S.; Achá, D.; Feng, X. B.; Gilmour, C. C.; Jonsson, S.; Mitchell, C. P. J. Challenges and opportunities for managing aquatic mercury pollution in altered landscapes. *Ambio* **2018**, *47* (2), 141−169.
(34) Cline, J. D. Spectrophotometric Determination of Hydrogen Sulfide in Natural Waters. *Limnol. Oceanogr.* **1969**, *14* (3), 454−458.
(35) Thomas, S. A.; Gaillard, J. F. Cysteine Addition Promotes Sulfide Production and 4-Fold Hg(II)-S Coordination in Actively Metabolizing *Escherichia coli*. *Environ. Sci. Technol.* **2017**, *51* (8), 4642−4651.
(36) Monperrus, M.; Tessier, E.; Veschambre, S.; Amouroux, D.; Donard, O. Simultaneous speciation of mercury and butyltin compounds in natural waters and snow by propylation and species-specific isotope dilution mass spectrometry analysis. *Anal. Bioanal. Chem.* **2005**, *381* (4), 854−862.
(37) Gilmour, C. C.; Elias, D. A.; Kucken, A. M.; Brown, S. D.; Palumbo, A. V.; Schadt, C. W.; Wall, J. D. Sulfate-Reducing Bacterium *Desulfovibrio desulfuricans* ND132 as a Model for Understanding

https://doi.org/10.1021/acsearthspacechem.4c00327
ACS Earth Space Chem. XXXX, XXX, XXX−XXX

Bacterial Mercury Methylation. *Appl. Environ. Microb.* **2011**, *77* (12), 3938−3951.
(38) Perrot, V.; Bridou, R.; Pedrero, Z.; Guyoneaud, R.; Monperrus, M.; Amouroux, D. Identical Hg Isotope Mass Dependent Fractionation Signature during Methylation by Sulfate-Reducing Bacteria in Sulfate and Sulfate-Free Environment. *Environ. Sci. Technol.* **2015**, *49* (3), 1365−1373.
(39) Thomas, S. A.; Catty, P.; Hazemann, J. L.; Michaud-Soret, I.; Gaillard, J. F. The role of cysteine and sulfide in the interplay between microbial Hg(II) uptake and sulfur metabolism. *Metallomics* **2019**, *11* (7), 1219−1229.
(40) Manceau, A.; Lemouchi, C.; Enescu, M.; Gaillot, A. C.; Lanson, M.; Magnin, V.; Glatzel, P.; Poulin, B. A.; Ryan, J. N.; Aiken, G. R.; Gautier-Luneau, I.; Nagy, K. L. Formation of Mercury Sulfide from Hg(II)-Thiolate Complexes in Natural Organic Matter. *Environ. Sci. Technol.* **2015**, *49* (16), 9787−9796.
(41) Zhang, T.; Kucharzyk, K. H.; Kim, B.; Deshusses, M. A.; Hsu-Kim, H. Net Methylation of Mercury in Estuarine Sediment Microcosms Amended with Dissolved, Nanoparticulate, and Microparticulate Mercuric Sulfides. *Environ. Sci. Technol.* **2014**, *48* (16), 9133−9141.
(42) Graham, A. M.; Cameron-Burr, K. T.; Hajic, H. A.; Lee, C.; Msekela, D.; Gilmour, C. C. Sulfurization of Dissolved Organic Matter Increases Hg-Sulfide-Dissolved Organic Matter Bioavailability to a Hg-Methylating Bacterium. *Environ. Sci. Technol.* **2017**, *51* (16), 9080−9088.
(43) Moreau, J. W.; Gionfriddo, C. M.; Krabbenhoft, D. P.; Ogorek, J. M.; DeWild, J. F.; Aiken, G. R.; Roden, E. E. The Effect of Natural Organic Matter on Mercury Methylation by *Desulfobulbus propionicus* 1pr3. *Front. Microbiol.* **2015**, *6*, 1389.
(44) Slowey, A. J. Rate of formation and dissolution of mercury sulfide nanoparticles: The dual role of natural organic matter. *Geochim. Cosmochim. Acta.* **2010**, *74* (16), 4693−4708.
(45) Ravichandran, M.; Aiken, G. R.; Ryan, J. N.; Reddy, M. M. Inhibition of precipitation and aggregation of metacinnabar (mercuric sulfide) by dissolved organic matter isolated from the Florida Everglades. *Environ. Sci. Technol.* **1999**, *33* (9), 1418−1423.
(46) Gerbig, C. A.; Kim, C. S.; Stegemeier, J. P.; Ryan, J. N.; Aiken, G. R. Formation of Nanocolloidal Metacinnabar in Mercury-DOM-Sulfide Systems. *Environ. Sci. Technol.* **2011**, *45* (21), 9180−9187.
(47) Gondikas, A. P.; Jang, E. K.; Hsu-Kim, H. Influence of amino acids cysteine and serine on aggregation kinetics of zinc and mercury sulfide colloids. *J. Colloid Interface Sci.* **2010**, *347* (2), 167−171.
(48) Bakour, I.; Isaure, M. P.; Barrouilhet, S.; Goñi-Urriza, M.; Monperrus, M. Coupling fluorescent probes to characterize S-containing compounds in a sulfate reducing bacteria involved in Hg methylation. *Talanta Open* **2023**, *7*, 100228.
(49) Adediran, G. A.; Van, L. N.; Song, Y.; Schaefer, J. K.; Skyllberg, U.; Björn, E. Microbial Biosynthesis of Thiol Compounds: Implications for Speciation, Cellular Uptake, and Methylation of Hg(II). *Environ. Sci. Technol.* **2019**, *53* (14), 8187−8196.
(50) Liu, Y. R.; Lu, X.; Zhao, L. D.; An, J.; He, J. Z.; Pierce, E. M.; Johs, A.; Gu, B. H. Effects of Cellular Sorption on Mercury Bioavailability and Methylmercury Production by *Desulfovibrio desulfuricans* ND132. *Environ. Sci. Technol.* **2016**, *50* (24), 13335−13341.
(51) Benoit, J. M.; Gilmour, C. C.; Mason, R. P. Influence Of Sulfide On Solid Phase Mercury Bioavailability For Methylation By Pure Cultures Of Desulfobulbus propionicus. *Environ. Sci. Technol.* **2001**, *35* (1), 127−132.
(52) Benoit, J. M.; Gilmour, C. C.; Mason, R. P.; Heyes, A. Sulfide Controls on Mercury Speciation and Bioavailability to Methylating Bacteria in Sediment Pore Waters. *Environ. Sci. Technol.* **1999**, *33* (10), 1780−1780.
(53) Garcia-Calleja, J.; Cossart, T.; Pedrero, Z.; Santos, J. P.; Ouerdane, L.; Tessier, E.; Slaveykova, V. I.; Amouroux, D. Determination of the Intracellular Complexation of Inorganic and Methylmercury in *Cyanobacterium Synechocystis* sp. PCC 6803. *Environ. Sci. Technol.* **2021**, *55* (20), 13971−13979.
(54) Wang, Y. W.; Janssen, S. E.; Schaefer, J. K.; Yee, N.; Reinfelder, J. R. Tracing the Uptake of Hg(II) in an Iron-Reducing Bacterium Using Mercury Stable Isotopes. *Environ. Sci. Technol. Lett.* **2020**, *7* (8), 573−578.
(55) Gutensohn, M.; Schaefer, J. K.; Yunda, E.; Skyllberg, U.; Bjorn, E. The Combined Effect of Hg(II) Speciation, Thiol Metabolism, and Cell Physiology on Methylmercury Formation by *Geobacter sulfurreducens*. *Environ. Sci. Technol.* **2023**, *57* (18), 7185−7195.
(56) Zhang, L. J.; Kang-Yun, C. S.; Lu, X.; Chang, J.; Liang, X. J.; Pierce, E. M.; Semrau, J. D.; Gu, B. H. Adsorption and intracellular uptake of mercuric mercury and methylmercury by methanotrophs and methylating bacteria. *Environ. Pollut.* **2023**, *331*, 121790.
(57) Schaefer, J. K.; Morel, F. M. M. High methylation rates of mercury bound to cysteine by *Geobacter sulfurreducens*. *Nat. Geosci.* **2009**, *2* (2), 123−126.
(58) Karlsson, T.; Skyllberg, U. Bonding of ppb levels of methyl mercury to reduced sulfur groups in soil organic matter. *Environ. Sci. Technol.* **2003**, *37* (21), 4912−4918.
(59) Joe-Wong, C.; Shoenfelt, E.; Hauser, E. J.; Crompton, N.; Myneni, S. C. B. Estimation of Reactive Thiol Concentrations in Dissolved Organic Matter and Bacterial Cell Membranes in Aquatic Systems. *Environ. Sci. Technol.* **2012**, *46* (18), 9854−9861.
(60) Mishra, B.; Shoenfelt, E.; Yu, Q.; Yee, N.; Fein, J. B.; Myneni, S. C. B. Stoichiometry of mercury-thiol complexes on bacterial cell envelopes. *Chem. Geol.* **2017**, *464*, 137−146.

https://doi.org/10.1021/acsearthspacechem.4c00327
ACS Earth Space Chem. XXXX, XXX, XXX−XXX